Journal of Medicinal Chemistry

Article

A Common Pharmacophore for a Diverse Set of Colchicine Site Inhibitors Using a Structure-Based Approach

Tam Luong Nguyen, Connor McGrath, Ann R. Hermone, James C. Burnett, Daniel W. Zaharevitz, Billy W. Day, Peter Wipf, Ernest Hamel, and Rick Gussio

J. Med. Chem., **2005**, 48 (19), 6107-6116• DOI: 10.1021/jm050502t • Publication Date (Web): 23 August 2005

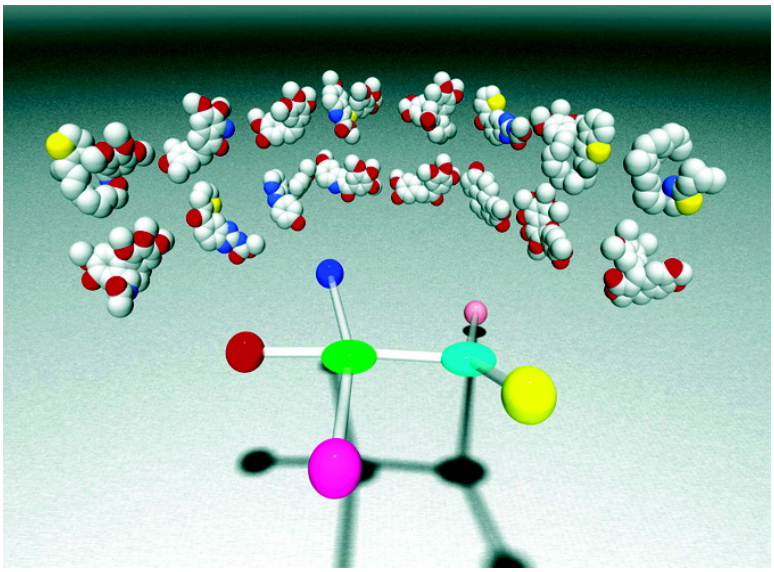

A Common Pharmacophore for a Diverse Set of Colchicine Site Inhibitors Using a Structure-Based Approach

Tam Luong Nguyen,*,† Connor McGrath,† Ann R. Hermone,† James C. Burnett,† Daniel W. Zaharevitz,† Billy W. Day,‡,§ Peter Wipf,§,|| Ernest Hamel,⊥ and Rick Gussio*,†

Target Structure-Based Drug Discovery Group, Developmental Therapeutics Program, National Cancer Institute, Frederick, Maryland 21702, Department of Pharmaceutical Sciences, University of Pittsburgh, Pittsburgh, Pennsylvania 15261, Department of Chemistry, University of Pittsburgh, Pittsburgh, Pennsylvania 15260, Center for Chemical Methodologies & Library Development, University of Pittsburgh, Pennsylvania 15260, and Screening Technologies Branch, Developmental Therapeutics Program, Division of Cancer Treatment and Diagnosis, National Cancer Institute, Frederick, Maryland 21702

Received May 27, 2005

Modulating the structure and function of tubulin and microtubules is an important route to anticancer therapeutics, and therefore, small molecules that bind to tubulin and cause mitotic arrest are of immense interest. A large number of synthetic and natural compounds with diverse structures have been shown to bind at the colchicine site, one of the major binding sites on tubulin, and inhibit tubulin assembly. Using the recently determined X-ray structure of the tubulin:colchicinoid complex as the template, we employed docking studies to determine the binding modes of a set of structurally diverse colchicine site inhibitors. These binding models were subsequently used to construct a comprehensive, structure-based pharmacophore that in combination with molecular dynamics simulations confirms and extends our understanding of binding interactions at the colchicine site.

Introduction

Microtubules are involved in a wide range of cellular functions and are critical to the life cycle of the cell. Composed of linear rows of alternating α- and β-tubulin, microtubules are highly dynamic and rapidly assemble and disassemble to meet the cell's needs.[1,2] Since inhibition of tubulin polymerization or blockage of microtubule disassembly increases the number of cells in metaphase arrest, microtubules are attractive molecular targets for anticancer therapeutics. Small molecules have been shown to bind at three major binding sites on tubulin: the vinca, taxane, and colchicine sites.[3,4] While drugs that act on the vinca and taxane sites have well-established roles in the treatment of human cancers, the therapeutic potential of the colchicine site in cancer treatment has yet to be realized.

Colchicine was extracted from the poisonous meadow saffron *Colchicum autumnale L.* and was the first tubulin destabilizing agent to be discovered. Experimental data showed that colchicine binds to β-tubulin at its interface with α-tubulin,[5] resulting in inhibition of tubulin polymerization. This binding mode was recently confirmed by the determination of a 3.58 Å X-ray structure of αβ-tubulin complexed with *N*-deacetyl-*N*-(2-mercaptoacetyl)colchicine (DAMA-colchicine), which is a close structural analogue of colchicine[6] (PDB code 1SA0). In the same paper, Ravelli et al. also reported the 4.20 Å X-ray structure of the αβ-tubulin:podophyllotoxin complex[6] (PDB code 1SA1), showing that podophyllotoxin also binds at the colchicine site and with a similar orientation as DAMA-colchicine.

While colchicine has played a central role in elucidating the physical properties and biological functions of tubulin and microtubules, its high toxicity has limited its therapeutic application.[7] Although colchicine site agents share a general toxicity, the promise to discover therapeutically useful analogues has fueled continued research. Over the years, a large number of natural and synthetic small molecules have been identified as colchicine site inhibitors (CSIs). While the enormous molecular diversity evident among the CSIs is of benefit to drug design, since a wide variety of molecular scaffolds are available for optimization, this diversity presents a significant challenge to determining the essential structural features for activity. At present, a common pharmacophore for CSIs has not been determined.

In this paper, we employed docking studies and molecular dynamics simulations to construct binding models for a set of structurally diverse CSIs, using the αβ-tubulin:DAMA-colchicine X-ray structure as the template. Examination of the binding models revealed a common pharmacophore not only for the CSIs in our set, but potentially, also for CSIs as a whole. Additionally, analyses of the docking trajectories of the ligands as they entered the colchicine site revealed critical intra- and intermolecular interactions that may affect their inhibitory properties.

Experimental Section

General. The Biopolymer, Discover and InsightII (Accelrys, San Diego, CA) programs were used to build and visualize the models. All simulations were performed using the CFF91 force-

* To whom correspondence should be addressed. Tel: 301-846-5791. Fax: 301-846-6106. E-mail:gussio@ncifcrf.gov (R. Gussio); Tel: 301-846-6035. Fax: 301-846-6106. E-mail: nguyent@ncifcrf.gov (T. L. Nguyen).

† Developmental Therapeutics Program, National Cancer Institute.

‡ Department of Pharmaceutical Sciences, University of Pittsburgh.

§ Department of Chemistry, University of Pittsburgh.

|| Center for Chemical Methodologies & Library Development, University of Pittsburgh.

⊥ Division of Cancer Treatment and Diagnosis, National Cancer Institute.

10.1021/jm050502t CCC: $30.25
Published on Web 08/23/2005

field with the nonbonded interaction limited to 13 Å and a distance-dependent dielectric constant. As implemented in Insight II, the HINT program (eduSoft, Richmond, VA) was used to evaluate the hydropathic quality of the protein−ligand interactions. HINT provides intuitively reasonable atom−atom interaction models and was employed using an exp $(-1r)$ distance dependence for hydropathic constants on atom pair interactions. The distance function was set to 50% hydropathic and 50% steric, where the steric term was a Lennard-Jones 6−9 function that is compatible with the CFF91 force-field. Lone pairs for basic atoms were vector focused by a factor of 10. HINT generates profiles consisting of a summation of the hydropathic interactions between all atom pairs in a molecule in a given molecular geometry. Hydropathic interactions are divided into six main classes. The "favorable" classes consist of hydrogen bonds, acid/base, and hydrophobic interactions, while acid/acid, base/base, and hydrophobic/polar interactions are the "unfavorable" categories. Each potential type from the CVFF database has a corresponding hydrophobic constant a_i derived from the hydrophobic fragment constant approach of Hansch and Leo.[8,9] This methodology reduces the empirical information from bulk molecular solvent partitioning to discrete atom−atom interactions. The hydropathic interaction value for an atom pair b_{ij} is a function of the hydrophobic constants for each atom, the distance between each of the atoms and the solvent accessible surface area (SASA) of the two atoms:

$$b_{ij} = s_i a_i s_j a_j R_{ij}$$

The distance function in the form $R_{ij} = e^{-r}$ has been reported to give a good fit to the published Leo polar proximity factors.[9] The SASA for atoms, s_i, is taken from literature values for proteins.[10] The interaction values, b_{ij}, for each atom pair are summed in one of the six aforementioned categories. Atom pairs within an amino acid residue, atoms that were bonded to each other, and atoms that were involved in 1−3 interactions were not included in the summation. A van der Waals component is also computed for each atom pair using published Lennard−Jones parameters. This penalizes atom−atom interactions which are too close in a manner independent from the hydropathic interaction.

Structure Preparation. The X-ray structure of the αβ-tubulin:DAMA-colchicine complex was used in this study. To begin, the stathmin-like domain and subunits C and D were removed. GDP, GTP, and DAMA-colchicine were fixed in Cartesian space. Hydrogen atoms were added and energy refined. Subsequently, a tethering force of 2000 kcal/mol Å^2 was applied to the heavy atoms of αβ-tubulin. Multiple cycles of minimization were performed with the tethering force on the side chain heavy atoms stepped off by a factor of 0.30 after each cycle until all external force was removed. The energy minimization involved up to 5000 steps of Fletcher−Powell optimization until the norm of the gradient was < 1.0 kcal/mol Å^2. Since the backbone heavy atoms were held in place by a strong tether, the refined model and the X-ray structure have the same secondary structures. A subset consisting of DAMA-colchicine, GTP, and residues from both α- and β-tubulin within 15 Å of the center of the colchicine site was created. To improve computational efficiency, this subset rather than the full αβ-tubulin model was used in this study.

The structure of colchicine **1** was derived from the X-ray structure of DAMA-colchicine, and podophyllotoxin **2** was obtained from its X-ray structure in complex with αβ-tubulin.[6] The structures of other small molecules were either obtained from the Cambridge Structural Database or were generated in the Biopolymer module of InsightII. If the configuration was not known, all stereoisomers were generated and studied. The ligands were energy minimized in the CFF91 force-field using the VA09A algorithm with a convergence criterion of 1.0×10^{-3} kcal/mol. At this stage, the ligands were at their local minima, which may not be their bioactive conformations.

Modeling the Bioactive Conformations. The bioactive conformations of **1** and **2** were delineated from the X-ray structures of DAMA-colchicine and podophyllotoxin in complex with αβ-tubulin.[6] The bioactive conformations of compounds **3**−**15** were determined in two stages.

In the first stage, the energy-minimized structures of **1**−**15** were aligned in a common orientation, using the structures of **1** and **2** as templates. This stage is ligand-based. Given that the trimethoxyphenyl (TMP) moieties of **1** and **2** occupy similar chemical space in the colchicine site, it is reasonable that the TMP moiety where it occurs would anchor the superimposition of **3**−**15**. However, a significant number of CSIs do not have the TMP moiety. Accordingly, two general approaches were employed to align **1**−**15**. The first approach involved ligands **3**, **4**, **5**, **6**, **7**, **8**, **13**, and **14**, which have the TMP group (TMP-ligands), and the second involves compounds **9**, **10**, **11**, **12**, and **15**, which do not have the TMP moiety (non-TMP-ligands). For the first approach, the TMP moieties of the TMP-ligands were superimposed onto that of **1**. With the centroids of the TMP moieties for **1** and the TMP-ligands tethered in Cartesian space, conformational sampling was employed to fit the remaining portion of each TMP-ligand to **1**, specifically to the hydrogen bond acceptor represented by the carbonyl group of the tropone ring, to the aromatic center represented by the tropone group and to the hydrophobic center represented by the methoxy group. In the second approach with compounds **9**, **10**, **11**, **12**, and **15**, non-TMP-ligands were segmented into regions and logP values were calculated. Regions of each ligand with logP values comparable to that of the TMP moiety were assumed to be its likely bioisostere. The centroids of the TMP moiety and the TMP-bioisostere were superimposed. As previously described, conformational sampling was used to fit the remaining portion of the non-TMP-ligand to **1**. The end result was a superimposition of **1**−**15**, aligned by their three-dimensional similarity.

In the second stage, the colchicine site model was used to refine the aligned conformations of **1**−**15**. This stage is structure-based. The limited molecular volume (10 Å × 10 Å × 4−5 Å) and the electrostatic surface contours of the colchicine site are severe constraints that limit the number of possible conformations for **1**−**15**, thus facilitating determination of their bioactive conformations. Using the αβ-tubulin:DAMA-colchicine complex as a template, aligned conformations of **1**−**15** were individually positioned in the colchicine site model. Although the binding modes of **1** and **2** have been experimentally determined via X-ray crystallography, these two compounds were also docked into our colchicine site model. During the docking of **1**−**15** into the colchicine site, van der Waals violations of 0.25 Å between tubulin and the CSI were removed using manual adjustments and energy refinement. The atoms of αβ-tubulin and GTP were fixed in Cartesian space, and molecular mechanics energy minimization was employed as described to find the nearest local minima of **1**−**15**. The ligand:tubulin interactions were hydropathically evaluated, and in instances where the hydropathic quality of the intermolecular interactions was significantly below that of the tubulin:DAMA-colchicine X-ray structure, iterative cycles of manual adjustment and energy minimization were performed. The end results were biochemically reasonable binding models for **1**−**15**. Consistent structural features and recurring protein−ligand interactions were identified in the binding models and were used to develop a structure-based pharmacophore.

Constrained Molecular Dynamics. To investigate the conformational behavior of the CSIs during docking, we used constrained molecular dynamics to undock the CSIs from the colchicine site in the binding models and reversed the resulting trajectories to provide a model of the binding event. Since the colchicine site is almost completely occluded in the binding model, residues of α-tubulin were removed to allow the ligands to exit the site during molecular dynamics simulations. A methane molecule served as a constraining target and was positioned ~40 Å from the aperture of the colchicine site, which is far enough away to not interfere with the exit of the ligand. The methane molecule and β-tubulin were fixed in Cartesian space. A distance constraint was created between the methane

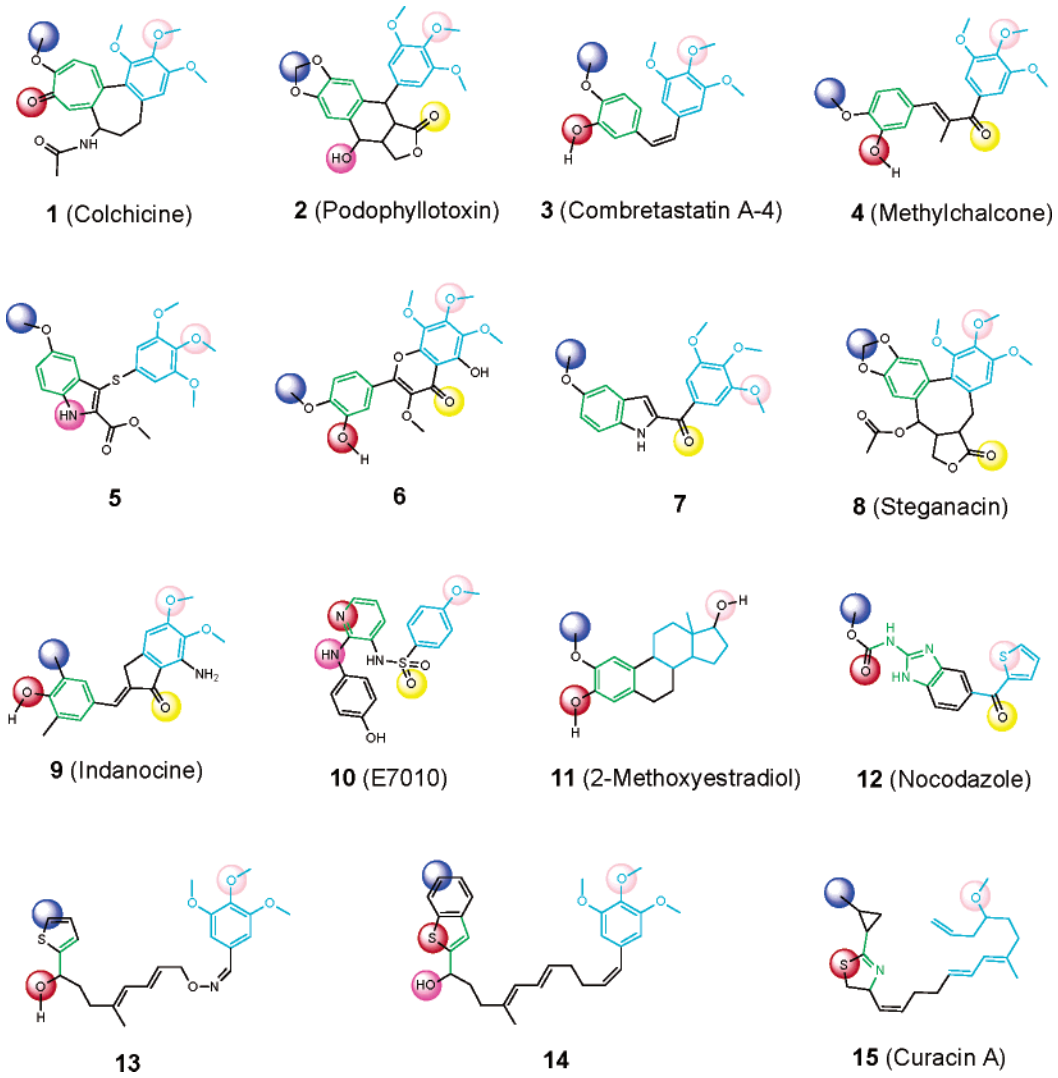

Figure 1. Two-dimensional structures of **1**−**15** with their common names given in parentheses. The red, pink, yellow, purple, and blue spheres represent pharmacophoric points A1, A2, A3, D1, and H1, respectively. The cyan and green lines denote the functional groups that comprise points H2 and R1, respectively. Points A1, A2, and A3 are hydrogen bond acceptors, D1 is a hydrogen bond donor, H1 and H2 are hydrophobic centers, and R1 is a planar group.

carbon atom and a heavy atom near the center of mass of the ligand. During molecular dynamics simulations, annealing, which entailed decreasing this distance constraint in 0.1 Å increments until the final distance of 20 Å, was enforced. At each 0.1 Å increment, molecular dynamics was performed for 600 fs with a time step of 0.2 fs at 300 K. Additionally, at each 0.1 Å increment, the coordinates were saved as a frame in the trajectory. The end result of the simulation was the complete undocking of the ligand from the colchicine site model. Reversing the trajectory generated the binding event.

The individual frames of the trajectories were analyzed using the HINT program. In a previous study,[11] it was found that the hydrophobic−polar (HP) term of HINT was the most useful in determining biochemically unrealistic contacts during docking. Accordingly, a trajectory frame function was developed in which the unfavorable HINT values for hydrophobic−polar interactions for all atom pairs from each frame were normalized within the trajectory using the maximum value for the trajectory:

$$\log \left| \frac{\sum_{i,j} \mathrm{HP}(i,j)_{frame}}{\sum_{i,j} \mathrm{HP}(i,j)_{\max}} \right|$$

Results and Discussion

Representative Set. The large number and molecular diversity of the CSIs is a major hurdle in the investigation of a common pharmacophore. Accordingly, in a preliminary study, we sought to establish if a common pharmacophore could be elucidated from a small set of CSIs (data not shown). To be useful, a representative set of CSIs must canvass the same chemical space as would any larger set of CSIs, and additionally must have a molecular diversity that is consistent with the topology and binding modes of any larger set of CSIs. Figure 1 shows the CSIs (compounds **1**−**15**) that we selected for our representative set. Since the binding modes of **1** and **2** have been previously determined by X-ray crystallography, these two compounds are the logical first choices for our representative set and provide a sound basis for elucidating the binding mode of other CSIs. Relative to **1** and **2**, compounds **3**−**15** were selected based on their molecular diversity and the uniqueness of their binding modes. To begin, candidate CSIs with distinct molecular scaffolds were identified in the literature. An array of topological descriptors (e.g., number of hydrogen bonding groups,

number of rotatable bonds, number of aromatic rings, number of atoms between rings, distribution of polar atoms within a molecule, etc.) were determined for the different candidate CSIs. While multiple topological parameters were used to select compounds **3**−**15**, parameters that describe conformational flexibility clearly delineate the molecular diversity of **1**−**15.** The conformational flexibility of a molecule can be assessed by the number of rotatable bonds, the number of aromatic rings, the number of double bonds, etc. Using these criteria, it is evident that a representative set of **1**−**15** consists of fairly rigid molecules such as **12** that has five rotatable bonds but exhibits conjugation between its rotatable bonds as well as flexible molecules such as compounds **13**−**15** that each have twelve rotatable bonds. In addition to diverse topology, a critical determinant in the selection of compounds **3**−**15** is the uniqueness of their binding modes. Due to the lack of empirical structural information on their binding modes, we employed exhaustive molecular docking on the candidate CSIs. The binding models of each CSI were determined by the steric and electrostatic features of the colchicine binding site and were used to assess the relative uniqueness of each CSI's binding mode. This was achieved in several ways. For instance, we examined the contacts between the candidate CSI and the tubulin structure within different distance ranges (see the table in the Supporting Information for residues that contact selected CSIs (compounds **1**−**15**) within 4.5 Å). Analyses of the binding models and the different topological descriptors indicate that compounds **1**−**15** suitably represent the molecular diversity and chemical space of the CSIs.

While structurally diverse, **1**−**15** fall into two general categories. The first category of CSIs (prototypical CSIs) is more structurally similar to colchicine. Compounds in this group have three classic features: (1) a diaryl system, (2) a trimethoxyphenyl (TMP) moiety, and (3) a constrained conformation. The second group of CSIs (atypical CSIs) lacks at least one of these features and consequently is more structurally diverse than the prototypical CSIs. Based on these definitions, **1**−**8** are prototypical and **9**−**15** are atypical. This balance in our set between prototypical and atypical CSIs was purposeful, providing us with a structural basis defined by the prototypical CSIs for exploring new chemical space with the atypical CSIs.

The binding modes of DAMA-colchicine, a close structural analogue of **1**, and **2** had previously been determined by X-ray crystallography[6] and, accordingly, provided the foundation for our work. The binding models of **1** and **2** presented here were energetically and hydropathically refined and have essentially the same conformation in the X-ray structures of DAMA-colchicine and **2**. Based on their structural similarity to **1**, the binding modes of **3**−**8** can be derived from docking experiments that use their common TMP moiety as a template. In fact, proposed binding modes for CSIs are beginning to appear in the literature.[12] In contrast, since the molecular structures of **9**−**15** are markedly different from **1**, determining their bioactive conformations is not as straightforward. For instance, while both **13** and **14** have TMP moieties that could be used to anchor their superposition with **1**, the two compounds also possess 12 rotatable bonds, 9 of which are outside of the TMP moiety, giving both compounds large conformational landscapes. As a result, after superimposing the TMP moieties, completing the fit of **13** and **14** to **1** was extraordinarily difficult. In fact, in a previous computational study,[13] **15**, which is also characterized by 12 rotatable bonds, was found to have only a minimal overlay with **1**. This is inconsistent with expectations, since both **1** and **15** bind tightly at the colchicine site, and highlights the fact that the bioactive conformations of highly flexible molecules, such as **13**−**15**, are notoriously difficult to determine in silico.

Architecture of the Colchicine Site. In their X-ray structures complexed with αβ-tubulin, DAMA-colchicine and **2** were unambiguously located in the electron density maps and found at the same site. The TMP moieties of DAMA-colchicine and **2** occupy similar Cartesian space and are buried in the β-tubulin structure near residue Cys β239. While the X-ray structure of the αβ-tubulin:DAMA-colchicine complex was selected for our study, similar results would have been obtained with the αβ-tubulin:**2** X-ray structure, since the two structures have an rms deviation of only 0.6 Å.

Figures 2A and 2B show the molecular volume of the colchicine site, which is illustrated as a surface rendering. The dimensions of the colchicine site are ∼10 Å × ∼10 Å × 4−5 Å. The colchicine site is located mostly in the β-subunit and is bordered in β-tubulin by helix 7, which contains Cys β239, and helix 8. Although not as extensively as β-tubulin, α-tubulin also forms crucial interactions at the colchicine site, notably the loop connecting sheet 5 and helix 5. The latter contains Thr α177 and Val α179, both of which appear to form hydrogen bonds to the CSIs. The molecular volume and electrostatic properties of the colchicine site are severe constraints on the conformations of the CSIs and, thus, proved useful in elucidating the bioactive conformations of **3**−**15**.

Binding Models. Figures 2C and 2D show the superimposed binding models of **1**−**15** in the colchicine site. Despite their strikingly different structures, **1**−**15** in the conformations shown in Figure 2C and 2D occupy similar Cartesian space in the colchicine site. As shown in Figure 2C, the TMP moieties or bioisostere equivalents are buried in the β-tubulin structure. Figure 2D shows a side view of the superimposition. Since the width of the colchicine site is only 4−5 Å, **1**−**15** are tightly held in the colchicine site. Two planes bisect the overlaid compounds and partition them into nearly-equal halves. The two planes are labeled A and B, have a tilt of ∼45°, and conform to the shape of the colchicine site. Since the prototypical CSI is a diaryl molecule, it is not unexpected that two planes characterized the docked conformations. However, this work showed that even among the CSIs that do not have the diaryl system, such as **15**, this biplanar architecture is conserved.

Figure 3 shows the individual binding models of **1**−**15**. The frequency of hydrogen bonds between the CSIs and tubulin are as follows: (1) in all 15 binding models, the CSI is hydrogen bonded to the thiol group of Cys β239; (2) in 11 of the 15 models, the CSI is hydrogen bonded to the backbone nitrogen atom of Val α179; (3) in eight binding models, molecular modeling indicates that structured water molecules and/or con-

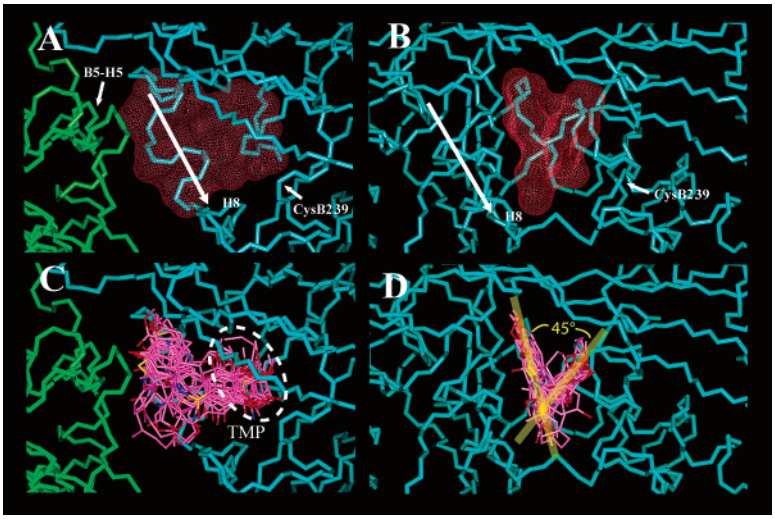

Figure 2. The molecular volume of the colchicine site as depicted in the molecular model and its occupancy by **1**−**15**. The peptide backbones of the tubulin dimer are rendered in stick with the α- and β-subunits colored green and cyan, respectively. For clarity, α-tubulin is not shown in B or D. (A) The volume of the colchicine site is highlighted by the orange grid lines. The colchicine site is located in the β-subunit and is bordered in β-tubulin by helix 7, which contains Cys β239, and helix 8 (labeled H8), which is denoted by a white solid line with the arrowhead at the amino terminus. Although not as extensive as with β-tubulin, α-tubulin forms critical interactions at the colchicine site. In particular, the loop connecting sheet 5 and helix 5 (labeled B5−H5), which contains Thr α177 and Val α179, appears to form hydrogen bonds to the CSIs. The colchicine site has dimensions of ∼10 Å × ∼10 Å × 4−5 Å. (B) Rotation of the view from A by 90° shows that the colchicine site has a narrow width of 4−5 Å. (C) The CSIs are rendered in stick and their carbon atoms are colored light purple, nitrogen atoms blue, oxygen atoms red, and sulfur atoms yellow. Hydrogen atoms are not shown. The binding models of **1**−**15** are overlaid in the colchicine site. The TMP moiety is buried in the β-tubulin structure. (D) Rotation of the view from C reveals that the docked conformations of **1**−**15** are bisected by two planes, which are separated by ∼45°.

formational changes in a loop structure would lead to hydrogen bonds between the CSI and the locus of hydrogen bond donors formed by the backbone nitrogen atoms of Ala β248, Asp β249, and Leu β250; (4) in four binding models, a hydrogen bond is formed between the CSI and the backbone oxygen atom of Thr α177.

Common Pharmacophore. The binding models of **1**−**15** were used to construct a common pharmacophore model. The consistent structural features and recurring tubulin−ligand interactions were the basis for the pharmacophoric points. We propose that the different structural classes of CSIs can be linked by a seven-point pharmacophore consisting of three hydrogen bond acceptors (A1, A2, and A3), one hydrogen bond donor (D1), two hydrophobic centers (H1 and H2), and one planar group (R1) (Figure 1). Three points A2, H2, and R1 are common to **1**−**15**, while H1 occurs in all except for **10**. This suggests that A2, H1, H2, and R1 are the essential features for activity. Additionally, while **1**−**15** are characterized by five to six points, none possesses all seven, suggesting that appropriate chemical modifications of **1**−**15** would result in more potent analogues. For instance, the binding affinity of **10**, which is characterized by six points, could be improved by methylation at the 5-position of the pyridine ring. This would provide the basis for point H1 and complete the seven-point pharmacophore.

Figure 4A depicts the seven pharmacophore points mapped onto the superimposition of **1**−**15** in the colchicine site. Clustered in the interior of the overlay, points H2 and R1, which are hydrophobic and planar groups, respectively, serve as the rigid portion of the molecular scaffold that satisfy the overall geometric and steric requirements of binding, while points A1, A2, A3, D1, and H1 form critical interactions with the protein and convey specificity to the binding. Similar to the three-dimensional structures of **1**−**15**, the seven pharmacophoric points can be partitioned among two planes (Figure 4B). Points A1, D1, H1, and R1 lie in plane A, and points A2, A3, and H2 lie in plane B. Relative to one another, the two planes have a tilt of ∼45° and match the shape of the colchicine site. Figure 4C shows the calculated distances between the pharmacophoric points. Points H2 and R1 that form the basis for the diaryl system in most CSIs are separated by 5.1 Å to 7.4 Å, while the other points are 2.3 Å to 10.7 Å apart. Figure 4D highlights the interaction of the pharmacophoric points with the tubulin structure. Hydrophobic center H1 is wedged between the side chains of Val α179 and Met β257. While H1 is typically represented by a methoxy carbon atom, H2 is often characterized by the TMP moiety. Thus, H2 is a significantly larger hydrophobic center than H1 and would likely drive ligand binding. Accompanying these hydrophobic contacts are six potential hydrogen bonds: (1) A1 to the amide nitrogen of Val α179 (A1−N distance of 3.3−4.6 Å), (2) A2 to the sulfur atom of Cys β239 (A2−S distance of 3.2−4.2 Å), (3−5) A3 to the amide nitrogen atoms of Ala β248, Asp β249, and Leu β250 (A3−N distance 3.9−6.4 Å), and (6) D1 to the carbonyl oxygen atom of Thr α177 (D1−O distance 3.0−4.9 Å). While the distance range of point A3 to the locus of hydrogen bond donors formed by the backbone nitrogen atoms of residues β248, β249, and β250 is significantly greater than expected for conventional hydrogen bonds, two factors suggest their presence. First, residues β248, β249, and β250 belong to the same loop structure, and conformational changes in this loop may bring this locus of hydrogen bond donors within hydrogen bonding distance of point A3. Second, molecular modeling indicates that structured

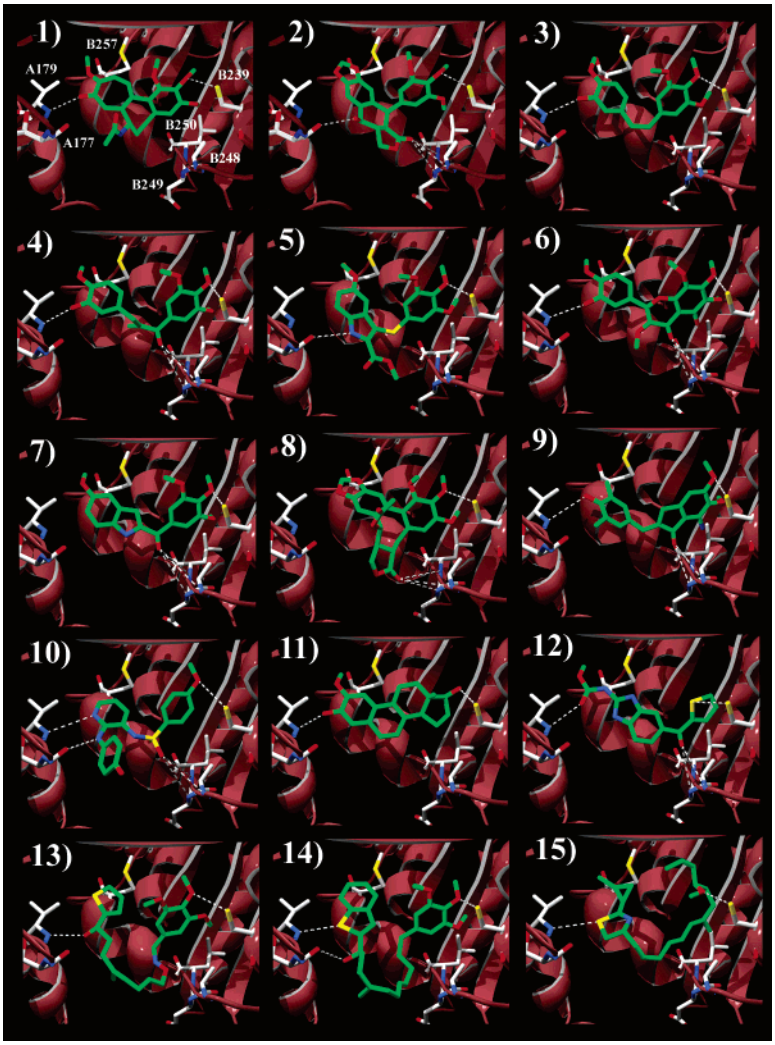

Figure 3. Binding models of **1**−**15**. The αβ-tubulin polypeptide backbones are rendered as brown ribbons. Residue side chains at the colchicine site (Thr α177, Val α179, Cys β239, Ala β248, Asp β249, and Leu β250), and **1**−**15** are shown in stick with the carbon atoms of tubulin colored white and the carbon atoms of the CSIs green. Nitrogen atoms are colored blue, oxygen atoms red, and sulfur atoms yellow. White dashed lines indicate potential intermolecular hydrogen bonds. The compound number is at the top left corner of each panel.

water molecules may mediate the interaction between point A3 and this locus of hydrogen bond donors (data not shown).

Binding Modes of Pharmacophoric Groups. Based on their common pharmacophoric points, we were able to classify **1**−**15** into seven groups (Table 1). By deconstructing the molecular structures of **1**−**15** into their common pharmacophoric features, these groups provide a powerful means of relating experimental data among the structurally different CSIs. Because only a sampling of possible CSIs is discussed in this paper, some of the groups contain a single compound. These single-compound groups are probably not special cases, and further studies should increase the number of compounds they contain.

Group I (A1-A2-H1-H2-R1 Pharmacophore). The A1-A2-H1-H2-R1 pharmacophore contains compounds **1**, **3**, **11**, **13**, and **15**. The molecular diversity of this group is apparent.

A variety of combretastatin-based analogues have been found to be antimitotic.[14−17] Using the binding model of **3**, it is possible to predict their bioactive conformations. Although structurally similar to **3**, phenstatin **16** (Figure 5) is more potent as an inhibitor of tubulin assembly.[18] The IC_{50}s for **3** and **16** are 1.0 μM and 0.4 μM, respectively. To explain this difference in activity, we constructed a binding model for **16**, using the model of **3** as a template (data not shown). The resulting model indicated that **3** and **16** belong to different pharmacophoric groups. A member of group V (A1-A2-A3-H1-H2-R1 pharmacophore), **16** has an additional hydrogen bond acceptor in point A3, and thus it could hydrogen bond via its carbonyl oxygen to the backbone N−H groups of residues β248-β249-β250. This additional hydrogen bond would explain the greater potency of **16** relative to **3**.

Various chemical substitutions at the 2- and 17-positions of **11** have been synthesized and evaluated for antimitotic activity.[19−23] A number of these analogues were shown to have comparable or improved antimitotic activity. Two of these are the 2-ethoxy congener **17**[19] and the 2-ethoxy-17-hydroxy-17-methyl congener **18** (Figure 5).[23] Using the docked conformation of **11** as a template, we constructed binding models for **17** and **18** (data not shown), and both are members of group I. However, consistent with experimental results, the

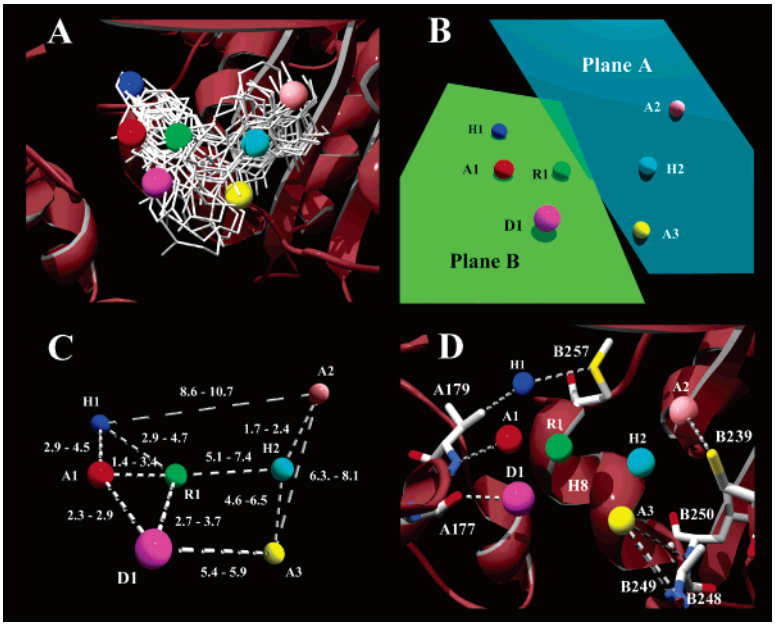

Figure 4. Mapping the pharmacophoric points. The pharmacophoric points are color coded as in Figure 1. The α- and *β*-tubulin polypeptide backbones are rendered as brown ribbons. (A) The docked conformations of **1**−**15** are shown as white sticks. The seven points of the pharmacophoric model are embedded in the overlay. (B) The seven points of the pharmacophoric model partition into two planes. Plane A (cyan) consists of points A2, A3, and H2, and plane B (green) points A1, D1, H1 and R1. (C) Based on the atom/centroid-atom/centroid distances of **1**−**15**, the distances between the pharmacophoric points were calculated in Å. D) Interactions between the pharmacophoric points and the tubulin structure. White dashed lines indicate potential intermolecular interactions. There are several hydrophobic contacts: (1) H1 to the side chains of Val α179 and Met *β*257, and (2) H2 to the side chains of Leu *β*255, Ala *β*316, Val *β*318 and Ile *β*378. Complementing these hydrophobic contacts are six potential hydrogen bonds: (1) A1 to the backbone nitrogen of Val α179, (2) A2 to the sulfur atom of Cys *β*239, (3) A3 to the backbone nitrogen of Ala *β*248, (4) A3 to the backbone nitrogen of Asp *β*249, (5) A3 to the backbone nitrogen of Leu *β*250, and (6) D1 to the backbone oxygen of Thr α177.

Table 1

CSI	points	group
1	A1-A2-H1-H2-R1	I
2	A2-A3-D1-H1-H2-R1	II
3	A1-A2-H1-H2-R1	I
4	A1-A2-A3-H1-H2-R1	V
5	A2-D1-H1-H2-R1	IV
6	A1-A2-A3-H1-H2-R1	V
7	A2-A3-H1-H2-R1	III
8	A2-A3-H1-H2-R1	III
9	A1-A2-A3-H1-H2-R1	V
10	A1-A2-A3-D1-H1-R1	VI
11	A1-A2-H1-H2-R1	I
12	A1-A2-A3-H1-H2-R1	V
13	A1-A2-H1-H2-R1	I
14	A1-A2-D1-H1-H2-R1	VII
15	A1-A2-H1-H2-R1	I

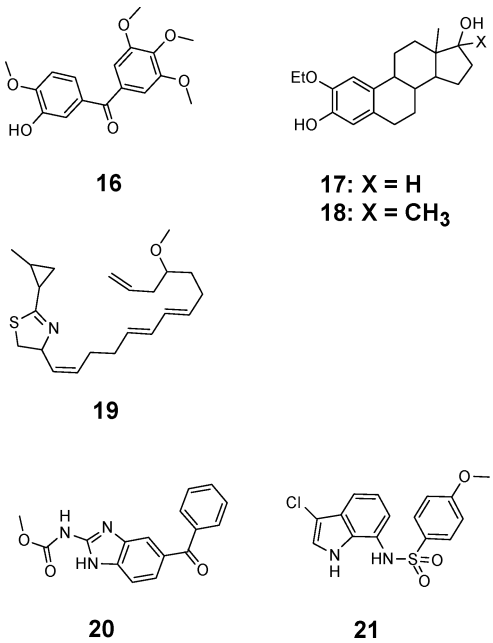

Figure 5. Two-dimensional structures of **16**−**21**.

binding model of **17** indicated that an ethyl group could be accommodated in the colchicine site without significant steric penalty. The added lipophilicity due to the ethyl group may explain the increased potency of **17**. The binding model of **18** demonstrated that small substitutions on opposite ends of the ligand can also be sterically and hydropathically accommodated in the colchicine site.

Compound **13** is a synthetic analogue of **15** that was designed to have the characteristics of the prototypical CSI.[24] The stereochemistry of the bioactive form of **13** has not been established. On the basis of the binding model of **13**, we propose that the (*R*)-hydroxyl, *cis*-oxime isomer is the more active form. In the (*R*)-isomer, the hydroxyl oxygen is 3.1 Å away from the backbone N−H group of Val α179 and is therefore likely hydrogen bonded, whereas in the (*S*)-isomer it is 4.0 Å away, further than expected for a typical hydrogen bond. In addition, the cis geometry of the oxime group allows the thiophene group of **13** to be overlaid with the tropone group of **1**, whereas the trans geometry places the thiophene group at the aperture of the colchicine site.

Compound **15** has an unusual structure for a potent CSI.[25−28] Using the binding model of **15** as a template, we docked a series of natural and synthetic analogues of curacin A and determined that, in general, they

confirmed the binding mode of **15** proposed here. As an example, we compared the binding models of **15** and **19** (data not shown). While their molecular structures differ by only a single methyl group, **15** and **19** have significantly different IC_{50} values against tubulin polymerization, i.e., 0.72 μM and 4.8 μM, respectively. What role does this methyl group play? In the binding model of **15**, this critical methyl group packs favorably against a hydrophobic pocket formed by the side chains of Leu β240, Leu β250, and Leu β253. Lacking this crucial methyl group, **19** cannot fully exploit the hydrophobic interior of the colchicine site and thus is a weaker antimitotic agent. The intrinsic binding energy of a methyl group in a drug-receptor interaction has been calculated to be 0.8 kcal/mol, but the binding energy can exceed this average value if the drug is sterically and electronically optimized for the receptor.[29] Accordingly, this methyl group of **15** may provide critical stability to ligand binding.

Group II (A2-A3-D1-H1-H2-R1 Pharmacophore). The A2-A3-D1-H1-H2-R1 group currently contains only **2**; however, its closely related congeners may belong to this group.[30]

Group III (A2-A3-H1-H2-R1 Pharmacophore). Compounds **7** and **8** comprise the A2-A3-H1-H2-R1 pharmacophore. The structure−activity data for a series of 2-aroylindoles suggest that the TMP moiety of **7** is not essential, but instead its activity depended upon substitution at the 3-position. This substituent is typically a methoxy group[31] (Figure 1). Compound **8**[32] has a similar molecular structure as **2**, but belongs to a different pharmacophoric group due to the absence of an appropriately positioned hydrogen bond donor.

Group IV (A2-D1-H1-H2-R1 Pharmacophore). Compound **5** is the only member of the A2-D1-H1-H2-R1 pharmacophore group. De Martino et al. recently proposed a binding model for **5** using the X-ray structure of the tubulin:DAMA-colchicine complex as a template.[12] We generated nearly the same binding model via an independent approach. In the two binding models, the TMP moieties of **1** and **5** adopt similar orientations near Cys β239 in the colchicine site.

Group V (A1-A2-A3-H1-H2-R1 Pharmacophore). The A1-A2-A3-H1-H2-R1 pharmacophore contains compounds **4**, **6**, **9**, and **12**. Although **4** is not a tricyclic system, the trans geometry of its ethenyl group gives **4** a similar conformation to that of the tricyclic compound **6**.

The binding model of **9** is consistent with the structure−activity data reported by Shih et al. for a series of indanone derivatives.[33] Additionally, the binding model may explain indanocine resistance in human leukemia. Recent biochemical and genetic analysis indicate that a single point mutation of Lys β350 to Asn on tubulin has a pronounced effect on indanocine toxicity.[34] In the binding model, the phenolic methyl group of **9** is 3.6 Å away from the C-γ atom of Lys β350 and forms a favorable hydrophobic contact. The point mutation of Lys β350 to Asn resulted in an unfavorable hydrophobic−polar contact between the methyl group of **9** and the side chain amide. This unfavorable interaction may explain the inability of **9** to bind to and inhibit assembly of tubulin containing the Lys350Asn mutant.

A series of nocodazole-like molecules were synthesized and evaluated for tubulin binding.[35] Nocodazole **12**[36] has a closely related structure in mebendazole **20**[37] (Figure 5). Docking studies of **12** and **20** suggest that the proton···π (arene) interaction contributes to their binding affinity. The π-clouds of the thiophene and phenyl rings can function as hydrogen bond acceptors and form a weak hydrogen bond when paired with a hydrogen bond donor such as the thiol group of Cys β239.

Group VI (A1-A2-A3-D1-H1-R1 Pharmacophore). At this time, compound **10** is the only compound in the A1-A2-A3-D1-H1-R1 pharmacophore. Sulfonamides have historically been of interest in drug development, and **10** has entered clinical trials as an orally active tubulin polymerization inhibitor.[38] Derived from the same drug lead as **10**, sulfonamide **21** was also shown to have antimitotic activity[39] (Figure 5). Docking studies of **21** using the binding model of **10** as template indicated that **21** belongs to group V. Compared to **10**, **21** has an additional hydrophobic center H1 in its chlorine atom, but it is missing hydrogen bond acceptor A1 and donor D1.

Group VII (A1-A2-D1-H1-H2-R1 Pharmacophore). Compound **14**[40] is the only member of A1-A2-D1-H1-H2-R1 pharmacophore group. The binding model of **14** indicated that the more active configuration is the (*R*)-hydroxyl, *cis*-ethenyl isomer. As noted above, compounds **13** and **14** belong to different pharmacophoric groups. While the hydroxyl functionality of **14** is amphipathic and could simultaneously function as a hydrogen bond acceptor and donor, in this instance, it is only a hydrogen bond donor, and paired with the backbone oxygen of Thr α177.

Pathway to the Colchicine Site. Using constrained molecular dynamics simulations, we undocked the CSIs from their binding models. The resulting trajectories were reversed to produce models of the binding event. The dynamic behaviors of the ligands in the simulations were examined to provide structural insights into their inhibitory properties that may not be apparent from their occupancy of the colchicine site. Here we present results of one such study on **13** and its congener **22**[24] (Figure 6A).

Experimental results indicate that **13** and **22** have significantly different abilities to inhibit colchicine binding, **13** inhibits 48% while **22** is essentially inactive, despite the two compounds displaying similar occupancy of the colchicine site (Figure 6B). Given that inhibition of colchicine binding is the result of **13** or **22** occupying the colchicine site, we studied the docking trajectories of **13** and **22** to explain their difference in activity. Figure 6C shows a plot of normalized unfavorable hydrophobic−polar values against time for **13** and **22**. During the simulation, the hydrophobic−polar interactions of **13** remained largely the same, indicating that there are few hindrances in its approach to the colchicine site. In contrast, the unfavorable hydrophobic−polar interaction of **22** spiked dramatically at 170 ps, the time in the simulation at which **22** approached the colchicine site. The unfavorable hydrophobic−polar value continued to rise for **22** until the 300 ps mark, at which point there was a steady decline in the hydrophobic−polar value. In the final docked conformation, **22** had approximately the same overall hydrophobic−polar score as **13**, a result

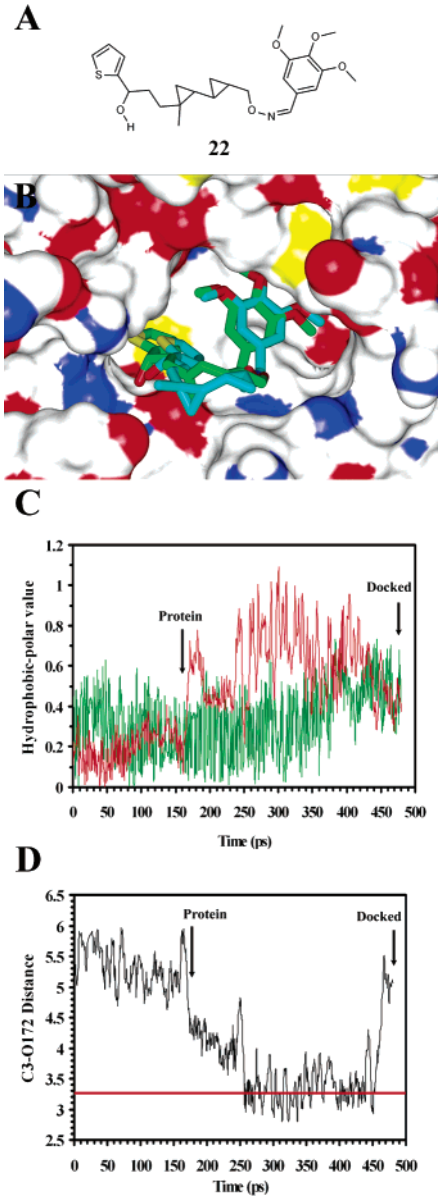

Figure 6. Molecular dynamics studies of the binding event of **13** and **22**. (A) Two-dimensional structure of **22**. (B) Overlay of the putative binding modes of **13** and **22** in the colchicine site. The surface rendering of the colchicine site is colored white for carbon and hydrogen atoms, blue for nitrogen, red for oxygen, and yellow for sulfur. The surface of α-tubulin is not shown. The stick renderings of **13** and **22** are colored blue for nitrogen atoms, red for oxygen atoms, yellow for sulfur atoms, green for the carbon atoms of **13**, and cyan for the carbon atoms of **22**. While **22** is significantly less active then **13**, the two compounds occupy similar steric and electrostatic space in the colchicine site. (C) A plot of the unfavorable hydrophobic−polar interaction as determined by the HINT program versus time in picoseconds for the molecular dynamics simulation of ligand docking. The green line represents values for **13** and the red line those for **22**. (D) A plot of the distance between the hydroxyl oxygen atom and the neighboring cyclopropyl carbon atom C-3 of **22** during the molecular dynamics simulation versus time in picoseconds. The red horizontal line at 3.25 Å indicates the sum of the van der Waals radii of carbon and oxygen atoms.

that is consistent with the similar predicted binding modes of the two compounds in the colchicine site.

A detailed analysis of the hydrophobic−polar values revealed that a specific interaction may be responsible for the spike in the unfavorable hydrophobic−polar score of **22**, specifically, the intramolecular interaction between the hydroxyl and cyclopropyl groups of **22**. The distance between the hydroxyl oxygen atom and the neighboring cyclopropyl C-3 carbon atom of **22** dropped dramatically at 170 ps, and between 200 ps to 400 ps, it was consistently <3.25 Å, which is the sum of the van der Waals radii of the carbon and oxygen atoms. At 450 ps, as **22** approaches its final docked position, this distance increased to >5 Å. The total energy of the conformation at 300 ps is ∼50 kcal/mol greater than that of the conformation at the nearest local minima. This energy difference confirms the unfavorable nature of the hydroxyl−cyclopropyl interaction.

By combining constrained molecular dynamics and hydropathic analyses, we present a new paradigm for investigating ligand binding. We are currently studying the binding events of other colchicine site inhibitors and their inactive congeners to provide a structural rationale for differences in activity. While a powerful tool, this combination of simulation and hydropathic analyses does have its limitations. For instance, it is not possible to determine the rates of association and dissociation between ligand and protein, since the factors that contribute to the on- and off-rates cannot be reasonably simulated.

Conclusion

We employed docking studies to construct biochemically reasonable binding models for a set of structurally diverse CSIs. A common pharmacophore model that links the multiple structural classes of CSIs was derived from these binding models, and it delineates the essential structural and functional features for inhibition. While the pharmacophore consists of seven points (three hydrogen bond acceptors, one hydrogen bond donor, two hydrophobic centers, and one planar group), none of the CSIs studied here was characterized by all seven pharmacophoric points. This suggests that the binding affinity of each chemotype can be improved by appropriate chemical modifications. In this way, the binding models and pharmacophore may provide useful insights for rational structure-based drug design.

Acknowledgment. The authors thank the Advanced Biomedical Computing Center at the National Cancer Institute for technical assistance and computing time on the SGI cluster. The content of this publication does not necessarily reflect the views or policies of the Department of Health and Human Services nor does mention of trade names, commercial products, or organization imply endorsement by the US Government.

Supporting Information Available: Coordinates of the binding models of **1**−**15**. Table showing residues within 4.5 Å of compounds **1**−**15** in their respective binding models. This material is available free of charge via the Internet at http://pubs.acs.org.

References

(1) Downing, K. H.; Nogales, E. Tubulin structure: insights into microtubule properties and functions. *Curr. Opin. Struct. Biol.* **1998**, *8*, 785−791.
(2) Downing, K. H.; Nogales, E. New insights into microtubule structure and function from the atomic model of tubulin. *Eur. Biophys. J.* **1998**, *27*, 431−436.

(3) Jordan, A.; Hadfield, J. A.; Lawrence, N. J.; McGown, A. T. Tubulin as a target for anticancer drugs: agents which interact with the mitotic spindle. *Med. Res. Rev.* **1998**, *18*, 259−296.
(4) Cragg, G. M.; Newman, D. J. A tale of two tumor targets: topoisomerase I and tubulin: the Wall and Wani contribution to cancer chermotherapy. *J. Nat. Prod.* **2004**, *67*, 232−244.
(5) Bai, R.; Covell, D. G.; Pei, X. F.; Ewell, J. B.; Nguyen, N. Y. et al. Mapping the binding site of colchicinoids on β-tubulin. 2-Chloroacetyl-2-demethylthiocolchicine covalently reacts predominantly with cysteine 239 and secondarily with cysteine 354. *J. Biol. Chem.* **2000**, *275*, 40443−40452.
(6) Ravelli, R. B.; Gigant, B.; Curmi, P. A.; Jourdain, I.; Lachkar, S. et al. Insight into tubulin regulation from a complex with colchicine and a stathmin-like domain. *Nature* **2004**, *428*, 198−202.
(7) Nakagawa-Goto, K.; Chen, C. X.; Hamel, E.; Wu, C. C.; Bastow, K. F. et al. Antitumor agents. Part 236: Synthesis of water-soluble colchicine derivatives. *Bioorg. Med. Chem. Lett.* **2005**, *15*, 235−238.
(8) Panthananickal, A.; Hansch, C.; Leo, A. Structure−activity relationship of aniline mustards acting against B-16 melanoma in mice. *J. Med. Chem.* **1979**, *22*, 1267−1269.
(9) Kellogg, G. E.; Semus, S. F.; Abraham, D. J. HINT: a new method of empirical hydrophobic field calculation for CoMFA. *J. Comput. Aided Mol. Des.* **1991**, *5*, 545−552.
(10) Shrake, A.; Rupley, J. A. Environment and exposure to solvent of protein atoms. Lysozyme and insulin. *J. Mol. Biol.* **1973**, *79*, 351−371.
(11) McGrath, C. F.; Tawa, G. J.; Luke, B. T.; Kellogg, G. E.; Zaharevitz, D. W. et al. A 3D-QSAR of pyridinone binding at the nonnucleoside binding site of HIV-1 reverse transcriptase: A hydropathic molecular dynamics approach. Presented at the 216th American Chemical Society National Meeting; Aug 23−27, 1998, Boston, MA.
(12) De Martino, G.; La Regina, G.; Coluccia, A.; Edler, M. C.; Barbera, M. C. et al. Arylthioindoles, potent inhibitors of tubulin polymerization. *J. Med. Chem.* **2004**, *47*, 6120−6123.
(13) Verdier-Pinard, P.; Lai, J. Y.; Yoo, H. D.; Yu, J.; Marquez, B. et al. Structure−activity analysis of the interaction of curacin A, the potent colchicine site antimitotic agent, with tubulin and effects of analogues on the growth of MCF-7 breast cancer cells. *Mol. Pharmacol.* **1998**, *53*, 62−76.
(14) Pettit, G. R.; Grealish, M. P.; Jung, M. K.; Hamel, E.; Pettit, R. K. et al. Antineoplastic agents. 465. Structural modification of resveratrol: sodium resverastatin phosphate. *J. Med. Chem.* **2002**, *45*, 2534−2542.
(15) Wang, L.; Woods, K. W.; Li, Q.; Barr, K. J.; McCroskey, R. W. et al. Potent, orally active heterocycle-based combretastatin A-4 analogues: synthesis, structure−activity relationship, pharmacokinetics, and in vivo antitumor activity evaluation. *J. Med. Chem.* **2002**, *45*, 1697−1711.
(16) Lin, C. M.; Singh, S. B.; Chu, P. S.; Dempcy, R. O.; Schmidt, J. M. et al. Interactions of tubulin with potent natural and synthetic analogues of the antimitotic agent combretastatin: a structure−activity study. *Mol. Pharmacol.* **1988**, *34*, 200−208.
(17) Borrel, C.; Thoret, S.; Cachet, X.; Guenard, D.; Tillequin, F. et al. New antitubulin derivatives in the combretastatin A4 series: synthesis and biological evaluation. *Bioorg. Med. Chem.* **2005**, *13*, 3853−3864.
(18) Liou, J. P.; Chang, J. Y.; Chang, C. W.; Chang, C. Y.; Mahindroo, N. et al. Synthesis and structure−activity relationships of 3-aminobenzophenones as antimitotic agents. *J. Med. Chem.* **2004**, *47*, 2897−2905.
(19) Cushman, M.; Mohanakrishnan, A. K.; Hollingshead, M.; Hamel, E. The effect of exchanging various substituents at the 2-position of 2-methoxyestradiol on cytotoxicity in human cancer cell cultures and inhibition of tubulin polymerization. *J. Med. Chem.* **2002**, *45*, 4748−4754.
(20) Cushman, M.; He, H. M.; Katzenellenbogen, J. A.; Varma, R. K.; Hamel, E. et al. Synthesis of analogues of 2-methoxyestradiol with enhanced inhibitory effects on tubulin polymerization and cancer cell growth. *J. Med. Chem.* **1997**, *40*, 2323−2334.
(21) Cushman, M.; He, H. M.; Katzenellenbogen, J. A.; Lin, C. M.; Hamel, E. Synthesis, antitubulin and antimitotic activity, and cytotoxicity of analogues of 2-methoxyestradiol, an endogenous mammalian metabolite of estradiol that inhibits tubulin polymerization by binding to the colchicine binding site. *J. Med. Chem.* **1995**, *38*, 2041−2049.
(22) Verdier-Pinard, P.; Wang, Z.; Mohanakrishnan, A. K.; Cushman, M.; Hamel, E. A steroid derivative with paclitaxel-like effects on tubulin polymerization. *Mol. Pharmacol.* **2000**, *57*, 568−575.
(23) Edsall, A. B.; Mohanakrishnan, A. K.; Yang, D.; Fanwick, P. E.; Hamel, E. et al. Effects of altering the electronics of 2-methoxyestradiol on cell proliferation, on cytotoxicity in human cancer cell cultures, and on tubulin polymerization. *J. Med. Chem.* **2004**, *47*, 5126−5139.
(24) Wipf, P.; Reeves, J. T.; Balachandran, R.; Day, B. W. Synthesis and biological evaluation of structurally highly modified analogues of the antimitotic natural product curacin A. *J. Med. Chem.* **2002**, *45*, 1901−1917.
(25) Wipf, P.; Xu, W. Total synthesis of the antimitotic marine natural product (+)-curacin A. *J. Org. Chem.* **1996**, *61*, 6556−6562.
(26) Wipf, P.; Reeves, J. T.; Day, B. W. Chemistry and biology of curacin A. *Curr. Pharm. Des.* **2004**, *10*, 1417−1437.
(27) Verdier-Pinard, P.; Sitachitta, N.; Rossi, J. V.; Sackett, D. L.; Gerwick, W. H. et al. Biosynthesis of radiolabeled curacin A and its rapid and apparently irreversible binding to the colchicine site of tubulin. *Arch. Biochem. Biophys.* **1999**, *370*, 51−58.
(28) Blokhin, A. V.; Yoo, H. D.; Geralds, R. S.; Nagle, D. G.; Gerwick, W. H. et al. Characterization of the interaction of the marine cyanobacterial natural product curacin A with the colchicine site of tubulin and initial structure−activity studies with analogues. *Mol. Pharmacol.* **1995**, *48*, 523−531.
(29) Andrews, P. R.; Craik, D. J.; Martin, J. L. Functional group contributions to drug-receptor interactions. *J. Med. Chem.* **1984**, *27*, 1648−1657.
(30) Desbene, S.; Giorgi-Renault, S. Drugs that inhibit tubulin polymerization: the particular case of podophyllotoxin and analogues. *Curr. Med. Chem. Anti-Cancer Agents* **2002**, *2*, 71−90.
(31) Beckers, T.; Reissmann, T.; Schmidt, M.; Burger, A. M.; Fiebig, H. H. et al. 2-aroylindoles, a novel class of potent, orally active small molecule tubulin inhibitors. *Cancer. Res.* **2002**, *62*, 3113−3119.
(32) Sackett, D. L. Podophyllotoxin, steganacin and combretastatin: natural products that bind at the colchicine site of tubulin. *Pharmacol. Ther.* **1993**, *59*, 163−228.
(33) Shih, H.; Deng, L.; Carrera, C. J.; Adachi, S.; Cottam, H. B. et al. Rational design, synthesis and structure−activity relationships of antitumor (E)-2-benzylidene-1-tetralones and (E)-2-benzylidene-1-indanones. *Bioorg. Med. Chem. Lett.* **2000**, *10*, 487−490.
(34) Hua, X. H.; Genini, D.; Gussio, R.; Tawatao, R.; Shih, H. et al. Biochemical genetic analysis of indanocine resistance in human leukemia. *Cancer Res.* **2001**, *61*, 7248−7254.
(35) Kruse, L. I.; Ladd, D. L.; Harrsch, P. B.; McCabe, F. L.; Mong, S. M. et al. Synthesis, tubulin binding, antineoplastic evaluation, and structure−activity relationship of oncodazole analogues. *J. Med. Chem.* **1989**, *32*, 409−417.
(36) Mejillano, M. R.; Shivanna, B. D.; Himes, R. H. Studies on the nocodazole-induced GTPase activity of tubulin. *Arch. Biochem. Biophys.* **1996**, *336*, 130−138.
(37) Friedman, P. A.; Platzer, E. G. Interaction of anthelmintic benzimidazoles and benzimidazole derivatives with bovine brain tubulin. *Biochim. Biophys. Acta* **1978**, *544*, 605−614.
(38) Yokoi, A.; Kuromitsu, J.; Kawai, T.; Nagasu, T.; Sugi, N. H. et al. Profiling novel sulfonamide antitumor agents with cell-based phenotypic screens and array-based gene expression analysis. *Mol. Cancer Ther.* **2002**, *1*, 275−286.
(39) Owa, T.; Yokoi, A.; Yamazaki, K.; Yoshimatsu, K.; Yamori, T. et al. Array-based structure and gene expression relationship study of antitumor sulfonamides including *N*-[2-[(4-hydroxyphenyl)amino]-3-pyridinyl]-4-methoxybenzenesulfonamide and *N*-(3-chloro-7-indolyl)-1,4-benzenedisulfonamide. *J. Med. Chem.* **2002**, *45*, 4913−4922.
(40) Wipf, P.; Reeves, J. T.; Balachandran, R.; Giuliano, K. A.; Hamel, E. et al. Synthesis and biological evaluation of a focused mixture library of analogues of the antimitotic marine natural product curacin A. *J. Am. Chem. Soc.* **2000**, *122*, 9391−9395.

JM050502T